Available online at www.sciencedirect.com
SCIENCE DIRECT®
Polymer 44 (2003) 4325–4340
polymer
www.elsevier.com/locate/polymer

Relaxation mechanism in several kinds of polyethylene estimated by dynamic mechanical measurements, positron annihilation, X-ray and ^{13}C solid-state NMR

Masaru Matsuo[a,*], Yuezhen Bin[a], Chunye Xu[a], Lin Ma[a], Takahiko Nakaoki[b], Takenori Suzuki[c]

[a]*Department of Textile and Apparel Science, Faculty of Human Life and Environment, Nara Women's University, Nara 630-8263, Japan*
[b]*Department of Chemical Material Science, Faculty of Science and Technology, Ryukoku University, Ootsu City 520-2194, Japan*
[c]*Radiation Science Center of High Energy Accelerator Research Organization, 1-1Oho, Tsukuba Ibaraki 305-0801, Japan*

Received 29 November 2002; accepted 22 April 2003

Abstract

Relaxation processes of several kinds of polyethylene films and fibers with different molecular orientational degrees and crystallinities were extensively investigated by the dynamic mechanical relaxation, positron annihilation and ^{13}C nuclear magnetic relaxation (^{13}C NMR). From complex dynamic tensile modulus, the activation energies of α_1 and α_2 relaxations were determined to be 97–118 and 141–176 kJ/mol, respectively. The activation energy of β relaxation was 114–115 kJ/mol. These values were similar to those of α_1 relaxation reported already. For γ relaxation mechanisms, there existed two mechanisms, γ_1 and γ_2, the activation energies being 9–11 and 23–25 kJ/mol, respectively. The values were independent of the molecular orientation and crystallinity. The two local motions indicate that non-crystalline phase composes of two regions of non-crystalline phase, rubber-like amorphous phase and interfacial-like amorphous phase. From ^{13}C NMR measurements of ^{13}C longitudinal relaxation time for the non-crystalline phase, the activation energy was 20.7 kJ/mol. This value is close to the activation energy (23–25 kJ/mol) of the γ_2 relaxation estimated by the dynamic mechanical measurement. The result by ^{13}C NMR did not provide two kinds of activation energy, indicating combined influence of the two correlation times. Even so, the activation energies obtained by ^{13}C NMR indicated that the γ_2 relaxation mainly is due to the motion of the C–C central bond of a short segment (e.g. three to four CH_2) within interfacial-like amorphous phase. The γ and β relaxation peaks by the dynamic mechanical measurements corresponded to the first and second lifetime transition of *ortho*-positronium indicating, in turn, a drastic change in free volume by local mode relaxation.

Keywords: Relaxation mechanism; Polyethylene; Positron annihilation

1. Introduction

It is well-known that there exist three kinds of transitions for polyethylene. The analysis of the transitions have been estimated by measuring mechanical relaxation [1–11], dielectric relaxation [12–14] and nuclear magnetic relaxation [15–18]. Among the three transitions, the study by measuring mechanical relaxation has been mainly concentrated on the crystal relaxation (the α transition) of polyethylene prior to melting. Since the resolution of the transition into two components was first investigated by Nakayasu et al. [1], multiple types of crystalline relaxation mechanisms have been studied by various authors [2–11].

Stein et al. [19–22] and Kawai et al. [23–26] have proposed that rheo-optical studies may be used to investigate the nature of mechanical loss processes of semi-crystalline polymers in connection with the deformation mechanism of the structural units. They have studied the deformation mechanism of semi-crystalline polymers, e.g. spherulitic polyethylene films, by using dynamic X-ray diffraction and dynamic birefringence techniques. In terms of rheo-optical studies, Kawai et al. obtained the three kinds of activation energies of the (110) and (200) planes by the Arrhenius plots on constructing the master curves of complex stress-orientation coefficient functions as well as of dynamic crystal compliance functions measured beyond

* Corresponding author. Tel./fax: +81-742-20-3462.
E-mail address: m-matsuo@cc.nara-wu.ac.jp (M. Matsuo).

0032-3861/03/$ - see front matter © 2003 Elsevier Science Ltd. All rights reserved.
doi:10.1016/S0032-3861(03)00352-5

room temperature [24–26]. The values of three kinds of energies are independent of the crystal planes and the values are close to the three kinds of activation energies in bulk, respectively. They concluded the α and β transitions as follows: the α_1 mechanical dispersion is assigned to intra-lamellar grain boundary phenomena associated with reorientation of crystal grains within the orienting lamellae, involving two types of preferential rotations of the crystal grains about their own *a*- and *b*-axes, respectively, mostly at the polar and equatorial zones of the spherulites; the α_2 mechanical dispersion is assigned to intra-crystal lattice retardation phenomenon, as observed by the frequency dispersion of the complex dynamic crystal lattice compliance function, and be ascribed to smearing-out effect of the crystal lattice potential at the onset of rotational oscillations of polymer chains within the crystal grains; the β mechanical dispersion is assigned to inter-lamellar grain boundary phenomena associated with orientational and distortional dispersions of noncrystalline materials between orienting lamellae, as rigid body, within uniaxially deformed spherulites.

Apart from their analysis for randomly orientated system [19–24], the anisotropy of crystal relaxation was investigated as a function of draw ratio by use of undrawn and drawn films with various draw ratios up to 400-fold [27,28]. Superposition was adopted by a combination of horizontal and vertical shifts resulting in apparent master curves of the storage and loss modulus functions. The value associated with the α_1 relaxation decreases as a draw ratio increases but the value leveled off when the draw ratio was beyond 100. On the other hand, the component of the α_2 relaxation decreased with increasing the draw ratio and became zero at a draw ratio of 400. This means that the α_2 relaxation could not be observed, when the external excitation is parallel to the *c*-axis.

Recently, Hu and Schnidt-Rohr provided the information of the α mechanism by NMR and they also summarized the origin of extremely high drawability reported by a number of authors in relation to the α-relaxation chain mobility in the crystallites [29]. Furthermore, the detailed analysis concerning chain mobility was done for high density polyethylene (HDPE) and ultra-high molecular weight polyethylene (UHMWPE) in terms of chain diffusion between crystalline and amorphous phases by two-dimensional exchange ^{13}C NMR [30] as well as chain flips by dipolar ^{13}C NMR [16–18]. These results pointed out the occurrence and the rate of 180° chain flip motions in the crystalline region of HDPE and UHMWPE by dipolar ^{13}C NMR. They concluded that the jumps occur between two sites, with a rotation angle of 180° and with a jump rate of ~10/s at ambient temperature and activation energy for the 180° chain flip is 122 ± 20 kJ/mol [18]. This value is slightly higher than values of the α_1 mechanism and slightly lower than that of the α_2 mechanisms estimated for several kinds of polyethylene by dynamic X-ray [24–26].

Another interesting treatment has been done by Nitta et al. for the α, β and γ relaxations using metallocene catalyzed linear polyethylenes [31]. They pointed out that the α relaxation and melting temperature have similar functional dependence of the inverse lamellar thickness and the β dispersion associated with the non-crystalline phase is different between the branched and linear polyethylene specimens.

In spite of the detailed analysis of the α and β relaxation mechanisms, the analysis of the γ relaxation mechanisms has been done using several specimens with different crystallinity and molecular weight on the basis of temperature dependence of the loss modulus at a fixed frequency. Khanna et al. [32] pointed out that the peak of the loss modulus of the γ relaxation is sensitive to the kinds of polyethylene. The relaxation peak position for HDPE specimens appeared at −107 °C regardless of the density or thermal history, while it occurred at −111 and −114 °C for the linear and branched low density polyethylene (LDPE) specimens, respectively. The magnitude of the peak tended to decrease with increasing crystallinity. Based on their results, they pointed out that the γ relaxation involves the motion of a short chain segment in the amorphous phase. Actually, the γ relaxation was not observed for very long chain paraffin, *n*-$C_{94}H_{190}$ [33], and very pure *n*-Eicosane (20 carbon atom paraffin) single crystals [34]. However, detailed analysis has never been carried out in terms of activation energy obtained by the Arrhenius plots of logarithm of shift factor versus the reciprocal of the absolute temperature. This is due to the difficulty in producing the master curves of the storage modulus E' and the loss modulus E'', because the values of E' and E'' as a function of frequency was scattered at the temperature lower than 0 °C.

In addition to several reports for nuclear magnetic relaxation described before [15–18], recent development of ^{13}C NMR has also provided useful information to study local dynamics in bulk polymers associated with the glass transition [35–41]. The spin–lattice relaxation time (T_{1C}) as a function of temperature measurements have been done for several kinds of polyesters [38], poly(vinyl methyl ether) [39], poly(propylene oxide) and poly(ethylene oxide) [40], since the minimum value of T_{1C} can be observed at the temperature higher than room temperature. For polyethylene, T_{1C} measurements were carried out at temperatures <0 °C by using solution-crystallized and melt-crystallized films by Chen et al. in order to measure the activation energy [41]. The minimum value of T_{1C} appeared around −10.5 °C for the solution-crystallized specimen and around −30.5 °C for the melt-crystallized specimen. The corresponding activation energies were 21.7 and 15.6 kJ/mol, respectively. They concluded that molecular mobility concerning the dispersion at temperature <0 °C is due to the rapid *trans-gauche* transition. This conclusion, however, must be examined carefully.

Another interesting result were reported by Spiess et al. [30,42,43] in deuterium quadrupole studies. They

interpreted the line shapes in terms of rigid bonds, reorientation of C–D bonds moving between 2 sites separated by the tetrahedral angle, between 3 such sites, and, more general motion. In their interpretation, the 2 site jumps were analyzed as arising from kink advance, while the 3-site jumps, as arising from five bond crankshaft motion, based on the concept that rigid bonds, 2- and 3-site tetrahedral jumps have characteristic line shapes.

During the last decade, positron annihilation in polymers has been extensively studied and positron-annihilation lifetime spectroscopy has been recognized as a useful method for studying the characteristics of polymers. According to several reports [44–47], it may be expected that an increase in the concentration of trapped electrons at a low temperature enhances the intensity of the long-lived component of positronium (I_3). This has been explained by the relaxation of the polymer. Positron annihilation is used here to make clear the origin of the β and γ relaxations.

As discussed before, except Kawai's papers [23–26], most of the relaxation mechanisms for polyethylene have been estimated on the basis of the information obtained from only one instrumental technique. Accordingly, this paper mainly deals with analysis of the γ relaxation mechanisms of several kinds of polyethylene films by the three kinds of methods, dynamic mechanics, positron annihilation, and ^{13}C NMR. The two or three methods were adopted for the same specimen to estimate the relaxation mechanisms. In the analysis of dynamic mechanical relaxation, E' and E'' as a function of frequency were obtained carefully to obtain the master curves. Interestingly, the Arrhenius plots indicated the possibility that there exist two mechanisms for the γ relaxation. The molecular motion associated with local mode relaxation was estimated in terms of the intensity of the long-lived component and life time of positronium. Furthermore, for ^{13}C NMR, T_{1C} were measured as a function of temperature and the activation energy was determined from the minimum value of T_{1C} which appeared at −25 °C. The γ relaxation mechanism was analyzed on the basis of the three methods discussed above.

2. Experimental section

2.1. Sample preparation

Films and fibers of low molecular weight polyethylene (LMWPE) were used as specimens in this experiment. In order to prepare the films, a linear polyethylene with a viscosity average molecular weight $\bar{M}_v$ of 70,000 was calendered under different friction ratios of the rolls at a desired temperature between 100 and 135 °C. The films were drawn at a commercial establishment and the draw ratio of the calender film was determined as the friction ratios of the rolls in a company. On the other hand, monofilaments (undrawn fiber) of a linear polyethylene with $\bar{M}_v = 54,000$ were prepared by melt spinning under a desired cooling rate between 2 and 10 °C/min by another company. This company suggested to us that the structure produced when the temperature reaches 115 °C must be preserved by the rapid cooling in the first stage to assure high modulus such as 55 GPa. The filaments were drawn at temperatures above 70 °C as the second stage to promote the molecular orientation. The detailed know-how for preparing both the specimens has been kept at each company.

To prepare the branched polyethylene films with crystallinity <50%, samples were prepared by molding at 180 °C with Sumikasen G201($\bar{M}_v = 41,300$ and melt index = 2) and G808 ($\bar{M}_v = 20,700$ and melt index = 200). The degree of branching is roughly 2.5 CH_3/100 carbons.

2.2. Measurements

2.2.1. Visco-elastic measurements

The complex dynamic tensile moduli were measured at frequencies from 0.01 to 100 Hz over the temperature range from −150 to 130 °C by using a visco-elastic spectrometer (VES-F) obtained from Iwamoto Machine Co. Ltd. The length of the specimen between the jaws was 40 mm and the width was about 1.5 mm. During measurements, the specimen was subjected to a static tensile strain (about 0.1%) in order to place the sample in tension during the axial sinusoidal oscillation. The complex dynamic modulus was measured by imposing a small dynamic strain (about 0.05%) to ensure linear visco-elastic behavior of the specimen [27]. Here we must emphasize its difficult to obtain master curves of complex dynamic tensile modulus because the observed data were scattered. Accordingly, the same measurements were carried out several times by using the same specimen without removing the specimen from the jaws. During the measurements, the specimens were elongated by the axial sinusoidal oscillation during long time measurement when the measured temperature was beyond 120 °C. The elongation was not recovered when temperature returned to −150 °C to pursue the second measurement. Accordingly, the master curve was achieved by using the frequency dependence of the complex modulus measured in the limited temperature range from −150 to 110 °C for the linear polyethylene films and fibers with crystallinity <68%.

2.2.2. Positron annihilation

The positron annihilation experiments were carried out with a conventional fast–fast coincidence system having a time resolution of 270 ps full width at half maximum (FWHM). The time spectrometer was composed of two plastic scintillation detectors (40 mm ∅ × 40 mm Pilot-U mounted on a Hamamatsu H1949 photomultiplier), two differential constant fraction discriminators (ORTEC 583): one for start signals from 1.27 MeV γ-rays and the other one for stop signals from 0.511 MeV annihilation γ-rays, a

time-to-amplitude converter (ORTEC 4570), and a multichannel analyzer with a 1024 conversion gain (SEIKO 7800). The position source was prepared by depositing ca. 1.1 MBq (30 μCi) of aqueous ^{22}NaCl on a Kapton foil of 7 μm thickness and 10 × 10 mm area. The source was further sealed in a 3 μm Mylar foil and then sandwiched by two identical samples. The diameter of the spot of ^{22}Na source was ∅40 mm.

When the sample was kept in a vacuum cell, two counters had to be separated by 25 mm. When the samples with ^{22}Na source were removed from the cell and directly sandwiched by two counters, the separation between the two counters was 5 mm and the counting rate was increased to 7–8 million events in 1 h.

2.2.3. ^{13}C NMR measurements

NMR measurements were carried out for dry gel films with a Bruker MSL 200 spectrometer, operating at a static magnetic field of 4.7 T. A radio frequency of 50 MHz was used for detection of ^{13}C resonance. The magic-angle spinning rate was 3 kHz. The contact time in ^{13}C CP-MAS measurement was 1 ms. The chemical shifts were mainly determined from the higher field signal (29.5 ppm) of adamantane relative to tetramethylsilane (TMS). Spin–lattice relaxation times (T_{1C}) longer than several tens of seconds were estimated using the method developed by Torchia, while T_{1C} shorter than a few seconds were measured by the standard-recovery pulse sequence without cross-polarization (CP). ^{1}H DD/MAS ^{13}C NMR without CP was measured to obtain the spectrum containing partial or total contributions from the components in the structure, quantitatively.

2.3. Sample characterizations

2.3.1. Orientation factors

The orientation factors of the *a*-, *b*- and *c*-axes were estimated from the orientation distribution functions of the reciprocal lattice vectors of the (200), (020) and (002) planes by the X-ray measurements which were carried out by 12 kW rotating anode X-ray generator (RDA-rA). In order to check the validity of the values of the *c*-axes, the orientation factors of the *b*- and *c*-axes were estimated from the factors concerning the (110) and (200) planes by Wilchinsky's equation [48]. The factors of the *c*-axis obtained by the two methods were in good agreement. The second order orientation factor of the amorphous chain segments was obtained from the birefringence as estimated by subtraction of the crystalline contribution from the total birefringence, assuming simple additivity. The procedure for evaluating the intrinsic birefringence of crystalline and amorphous phases is described elsewhere [49]. Here we noted that the X-ray diffraction pattern showed circular diffraction rings, when the X-ray was directed parallel to the stretching direction (end view). This indicates that crystallites within all the specimens take a random orientation around the machine direction.

2.3.2. Melting point and crystallinity

The crystallinity was calculated from the density which was measured by a pycnometer in chlorobenzene–toluene as a medium, using 1.000 and 0.852 g/cm^3 as the densities of the crystal and amorphous phases, respectively [50]. The melting point was estimated in terms of melting endotherms of DSC curves obtained at a constant rate of 10 °C/min. Specimens, weighing 5 mg each, were placed in a standard aluminum sample pan.

3. Results and discussion

Table 1 shows the characteristics of the calender films with different draw ratios, undrawn and drawn fibers produced by melt spinning, and melt films prepared in our laboratory. In Table 1, the melting point, the volume crystallinity, birefringence, long period and the storage modulus of the calender films at 20 °C increases gradually with increasing draw ratio λ. The Hv light scattering from calender films showed X-type patterns whose lobes are extended in the horizontal direction, indicating existence of rod-like textures oriented preferentially in the stretching direction [51]. On the other hand, Hv scattering from the melt films shows four-leaf-clover type patterns indicating existence of spherulites [52]. The average radius estimated from a scattering angle taking the maximum intensity is 14 and 170 μm for the melt films G201 for G808 respectively. Here it is of interest to consider that the storage modulus of the drawn fiber is much higher than that of the drawn film with $\lambda = 14$, although the birefringence of the fiber is slightly lower than that of the drawn film.

Table 2 shows the orientation factors of the *a*-, *b*-, *c*-axes and the amorphous chain segments. With increasing draw ratio, the *c*-axes and amorphous chain segments orient predominantly in the machine direction and the orientational degree of the *c*-axes is more pronounced than that of the amorphous chain segments. For the undrawn fiber (monofilament), the *a*-axes take the preferential orientation with respect to the machine direction and the *b*-axes orient almost perpendicular. The *c*-axes and the amorphous chain segments of the drawn fiber orient preferentially in the stretching direction. In comparison with the values of the orientation factors in Table 2, the orientational degree of the *c*-axes of the drawn fiber is less pronounced than that of the drawn film with $\lambda = 14$, while the preferential alignment of the amorphous chain segments is slightly higher than that of the drawn film. By using the specimens with various characteristics listed in Tables 1 and 2, the α, β and γ relaxations are analyzed in terms of their activation energy.

Fig. 1 shows temperature dependence of the storage modulus E' and the loss modulus E'' at a frequency of 10 Hz for the calender films with $\lambda = 3$ and 14. As reported

Table 1
Characteristics of calender films with different draw ratios (λ), fibers produced by melt spinning and melt films

Specimens	Calender film				Fiber		Melt film	
	3	6	8	14	Mono-filament	Drawn	G201	G808
Melting point (°C)	133.0	133.2	134.1	135.0	134.0	141.5	108.0	105.1
Crystallinity (%)	70.6	72.1	73.9	78.6	68.4	86.4	45.6	45.9
Storage modulus at 20 °C (GPa)	2.71	3.98	4.30	15.30	1.85	55.6	0.17	0.13
Birefringence ($\times 10^{-3}$)	40.5	44.8	46.6	50.3	3.36	48.0	0	0
Long period (nm)	23.0			28.0			22.5	36.5

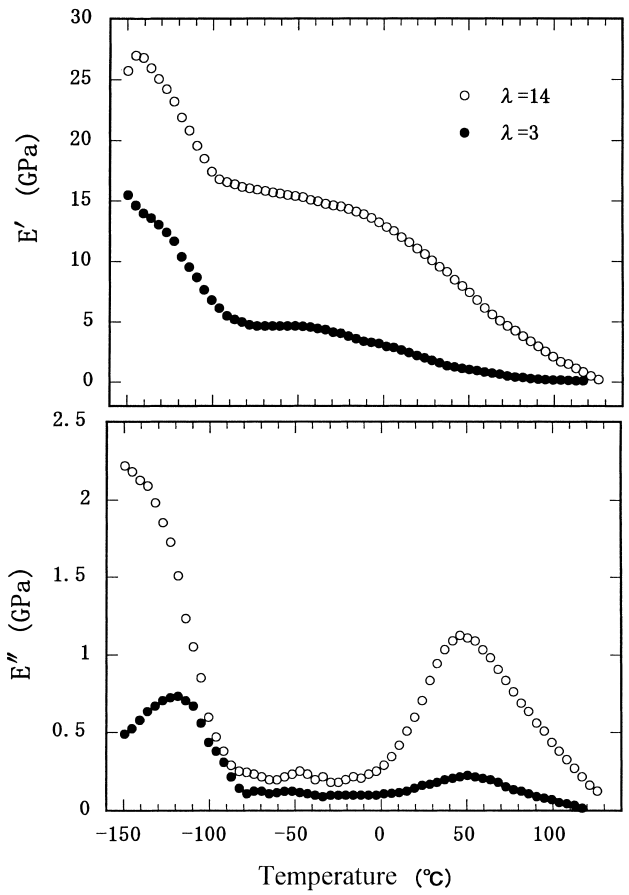

Fig. 1. Temperature dependence of the complex dynamic moduli at a frequency of 10 Hz for the calender films with λ = 3 and 14.

elsewhere [53], the loss modulus for the specimens shows the α and γ relaxations, while no β relaxation peak is observed because of the high crystallinity >70% of linear polyethylene. The measurements were done to know the approximate peak magnitude of several kinds of relaxation processes. Based on the results, the frequency dependence of E' and E'' was measured in the wide temperature range from −150 to 110 °C to pursue a detailed analysis of the α and γ relaxations.

Figs. 2 and 3 show the master curves of E' and E'' against frequency, respectively, for the calender films at λ = 3 and 14, which were reduced to the common reference temperature of 60 °C. Each curve is obtained by shifting horizontally and then vertically until a good superposition is achieved. It is seen that each master curve of E'' in Fig. 3 has two broad dispersion peaks at low and high frequency ranges, respectively. In comparison with the master curves reported for polyethylene elsewhere [26], it can be inferred that the broad peaks at low frequency corresponds to the overlapping of the α_1, α_2 and β relaxation peaks, while the broad peak at high frequency range corresponds to the γ relaxation peak. Here we must emphasize that the frequency dependence must be measured at temperature < −150 °C to achieve the full (perfect) broad master curve but this measurement is impossible in our instrument. Incidentally, even the broad peak of the master curve of E'' beyond $\log \nu_{aT} = 6$ shown in Fig. 3 has never been reported, because most of the measurements for frequency dependence were carried out above room temperature. Anyway, the broad dispersion peak corresponding to the γ relaxation at the high frequency range may be expected to consist of

Table 2
The second order orientation factors of three principle crystallographic axes and amorphous chain segments of calender films and fibers by melt spinning

Specimens	Calender film				Fiber	
	3	6	8	14	Mono-filament	Drawn
a-axis	−0.387	−0.435	−0.450	−0.476	0.245	−0.410
b-axis	−0.370	−0.391	−0.412	−0.453	−0.356	−0.434
c-axis	0.760	0.827	0.861	0.929	0.112	0.844
Amorphous chain segments	0.637	0.730	0.743	0.751	−0.048	0.824

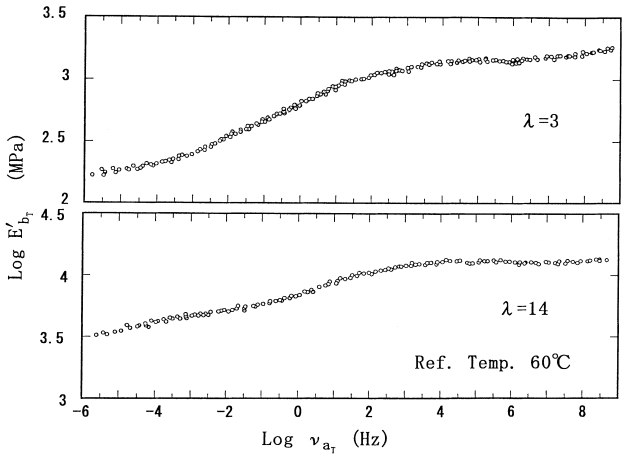

Fig. 2. Master curves of E' for the calender films with $\lambda = 3$ and 14.

more than two relaxation mechanisms. However, as discussed before, direct peak separation into the respective contributions was very difficult, since the data at log $\nu_{aT} > 8.5$ to obtain a perfect γ dispersion peak could not be obtained in our instrument.

In order to classify the broad dispersion curve of E'' in Fig. 3 into multiple components, the logarithm of the temperature dependence of the horizontal shift factor $a_T(T, T_o)$ was plotted against the reciprocal absolute temperature as shown in Fig. 4(a). The Arrhenius plots thus obtained are represented by four straight lines. The lines were drawn by the method of least squares. But the activation energies determined by the slopes of the drawn lines contains error because of the scattered plots. Of course, the values are confirmed to be within the experimental error. The activation energies obtained from the slopes of these lines are given as 10, 25, 110, and 150 kJ/mol for the specimen with $\lambda = 3$ and 11, 25, 108 and 148 kJ/mol for the specimen with $\lambda = 14$. These results clearly indicate that the dispersion curves of E' and E'' in Figs. 2 and 3 consist of four components. According to numerous previous studies, the estimated values of the activation energies are in the two ranges of the literature values of HDPE, i.e. from 98 [26] to

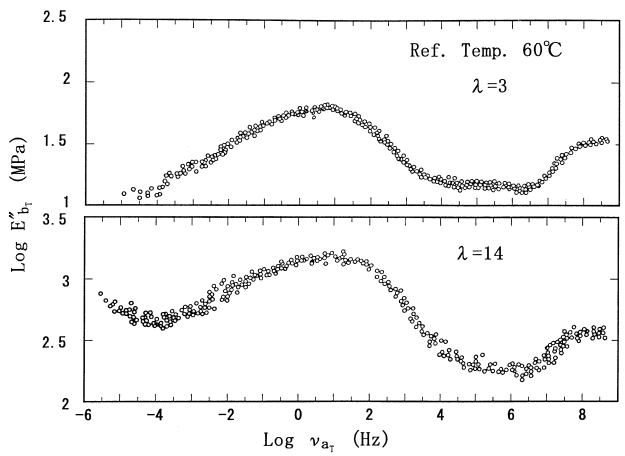

Fig. 3. Master curves of E'' for the calender films with $\lambda = 3$ and 14.

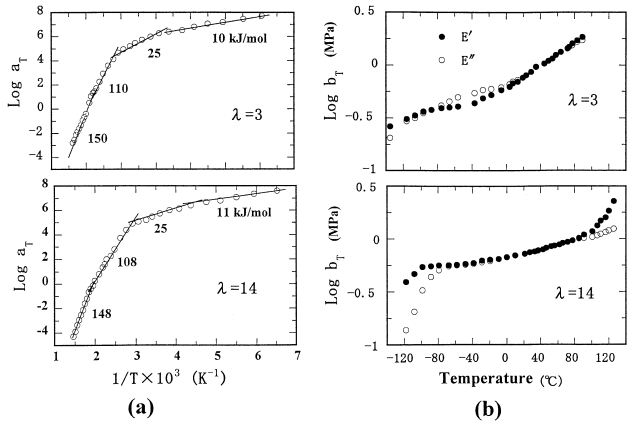

Fig. 4. (a) Arrhenius plots of the horizontal shift factor $a_T(T, T_o)$ and (b) the logarithm of the vertical shift factor $b_T(T, T_o)$ versus temperature for the calender films with $\lambda = 3$ and 14.

117 kJ/mol [1] for α_1 and 147 [27] to 193 kJ/mol [7,8] for α_2. Therefore, the activation energies of 110 and 108 kJ/mol correspond to the α_1 relaxation mechanism of the specimens with $\lambda = 3$ and 14, respectively, while those of 150 and 148 kJ/mol correspond to the α_2 dispersion. The activation energies of the α_1 and α_2 relaxations become smaller with increasing draw ratio.

Figs. 5 and 6 show the master curves of E' and E'', respectively, for the undrawn fiber (mono-filament) and drawn fiber. Each curve was obtained by shifting horizontally and then vertically until a good superposition was achieved as in the case of the calender films. The profiles in Figs. 5 and 6 are similar to those in Figs. 2 and 3. The broad dispersion curves may be expected to consist of several mechanisms. As discussed in the case of the master curves in Figs. 2 and 3, the direct separation of the reduced modulus into the respective contributions is also very difficult and consequently the relaxation mechanisms must be distinguished by the activation energies derived from the Arrhenius plots. The results are shown in Fig. 7(a). To carry out the superposition of E' and E'', the required vertical shift was necessary to obtain the master curves as shown in Fig.

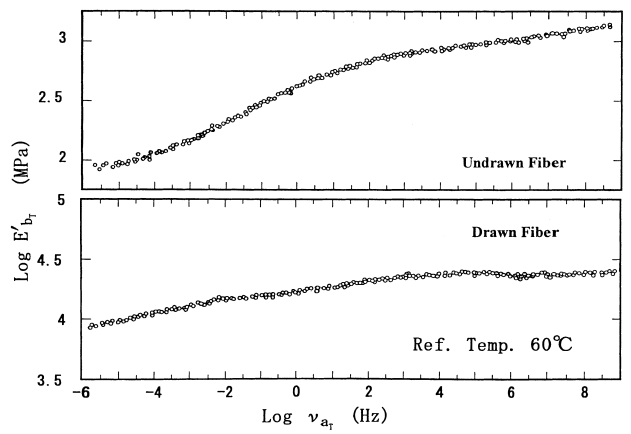

Fig. 5. Master curves of E' for the undrawn and drawn fibers.

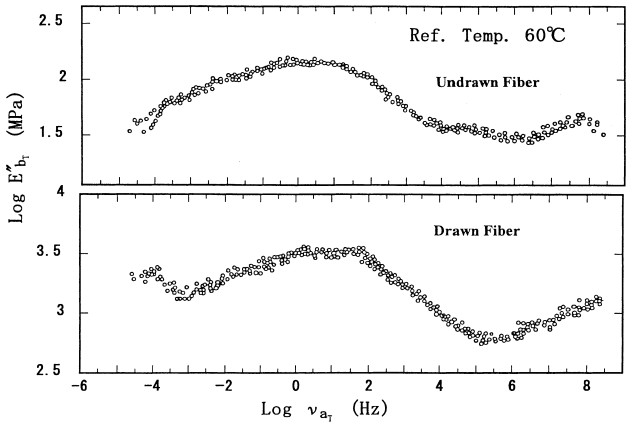

Fig. 6. Master curves of E'' for the undrawn and drawn fibers.

7(b) but the shift factor becomes smaller as the draw ratio increases.

The Arrhenius plots in Fig. 7(a) are represented by four straight lines. The activation energies obtained from the slopes of these lines are given as 176, 118, 24 and 9 kJ/mol for the undrawn fiber and 141, 97, 23 and 10 kJ/mol for the drawn fiber, indicating that each broad dispersion curve in Figs. 5 and 6 consists of the four components. Judging from the literature values, it is obvious that 176 and 141 kJ/mol corresponds to the α_2 dispersion, while 118 and 97 kJ/mol, the α_1 dispersion. The values for the α_1 and α_2 relaxation mechanisms become lower by elongation and this tendency is similar to the results for the calender films (see Fig. 4) and ultradrawn polyethylene [27]. Actually, the undrawn fiber with the preferential orientation of the *a*-axes (see Table 2) shows the large activation energy of the α_2 dispersion.

The remaining items of activation energies in Figs. 4(a) and 7(a) are thought to belong to the γ relaxation mechanism. Several controversies have been discussed already about the origin of the γ relaxation mechanism. We shall briefly summarize some references. For example, Illers proved that the γ peak is due to the amorphous fraction [53], while Hoffman et al. proposed that it is strictly due to defects in the crystalline phase [52]. Khanna et al. pointed out that the γ relaxation involves the motion of a short segment (e.g. three to four CH_2) belonging to the amorphous phase and the chain ends within amorphous fractions [32]. Their concept is based on the basis of the experimental results that the intensity of the γ peak tended to decrease with increasing crystallinity. These previous reports [32,53,54] indicate that the γ relaxation contains several local relaxation mechanisms. If this is the case, the results in Figs. 4(a) and 7(a) support the above concept. In Fig. 4(a), the two kinds of activation energies, 10–11 and 25 kJ/mol, associated with the γ relaxation are almost independent of the draw ratio. The tendency for the γ relaxation is different from that of the β mechanism [27], which supports the concept of Iller [53] and Khanna [32]. Judging from the two kinds of activation energies lower than those of the α and β mechanisms, it may be expected that the γ relaxation is essentially attributed to the local motion of central C–C bond of short chain segments and/or local motion of loose chain ends in the amorphous phase. If this is the case, the γ relaxation should be independent on the molecular orientational degree as well as the morphology of superstructure listed in Tables 1 and 2. In Fig. 7(a), the activation energies of the γ dispersion were 9–10 and 23–24 kJ/mol for undrawn and drawn fibers, respectively, indicating that the two kinds of activation energies of the γ dispersion are also independent of molecular orientation and crystallinity. The detailed analysis of the γ dispersion shall be discussed later in this paper.

Here it should be noted that vertical shift is significant in construction of the master curves. Fig. 4(b) shows the temperature dependence of the vertical shift factors

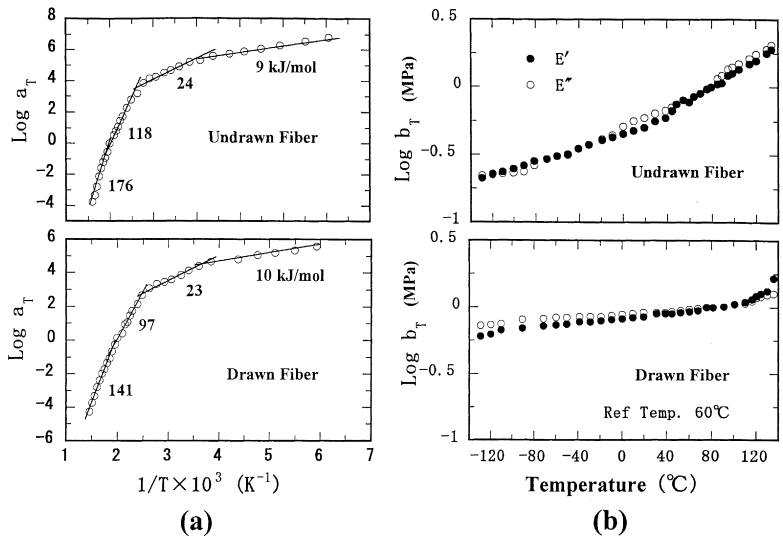

Fig. 7. (a) Arrhenius plots of the horizontal shift factor $a_T(T, T_o)$ and (b) the logarithm of the vertical shift factor $b_T(T, T_o)$ versus temperature for the undrawn and drawn fibers.

$b_T(T, T_o)$ of E' and E''. As can be seen in the figure, the temperature dependence of $b_T(T, T_o)$ in the temperature range from −80 to 82 °C is roughly given by a common straight line when plotted in logarithmic terms against a linear scale of temperature. Above 82 °C and below −80 °C, the relationship between $b_T(T, T_o)$ and T deviates from the straight line. The same tendency shall be represented later in Fig. 7(b). The necessity of the vertical shift and the derivation of straight line have been reported for several kinds of polyethylene films.

The significance of the vertical shift factor was discussed by Nagamatsu's [55] and Miki's [56,57] approaches. The former approach was based on the temperature dependence of amorphous entropic elasticity supplemented by the volume effect of the amorphous regions. On the other hand, the latter approach took into account the temperature dependence of crystal elasticity, based on a theory by Wada [58] and Okano [59], of a smearing-out effect on the intermolecular potential within a crystal lattice. Kawai et al. pointed out that both of the approaches give much smaller temperature dependence of the vertical shift factor than that required for fitting the experimental data [24–26]. They concluded that the shift factor is related to the temperature dependence of the crystal elasticity in the polar zone within polyethylene spherulites on the basis of the temperature dependence of the structural and mechanical parameters of the spherulitic model. If the concept by Kawai et al. is correct, the mechanical behavior of crystallites perpendicular to the chain axis is certainly due to the temperature dependence of crystal elasticity, since the crystal lattice modulus in the chain direction is independent of temperature below the normal melting point [60]. Accordingly, the shift factor becomes smaller with increasing draw ratio in the temperature range from −80 to 90 °C as shown in Figs. 4(b) and 7(b). As a typical example, the shift factor was very small for the ultra-drawn film with $\lambda = 400$ whose second order orientation factor is almost unity [27].

Here, we must consider another possibility that the γ relaxation involves that the number of carbons on the chain increase as temperatures rise and consequently it is not a simple process that only frequency is changing with temperature. The assumption of two kinds of γ relaxation, γ_1 and γ_2, satisfied the concept for two kinds of non-crystalline regions, rubber-like and interfacial-like components by ^{13}C NMR, which shall be discussed later. If this is the case, the evidence seems to point to a motion gradually increasing in complexity and therefore exhibiting gradual increasing in the activation energy.

To derive the more precise conclusion concerning the α, β, and γ relaxation in terms of their activation energies, similar estimation was done for the fibers with different molecular orientation modes and the characteristics of the fibers are shown in Table 1 together with other specimens. In doing so, as the preliminary experiments, the temperature dependence of E' and E'' at a frequency of 10 Hz was measured for the undrawn and drawn fibers. It was confirmed that the E'' behavior for the specimens with crystallinity >68% provides the α and γ relaxation peaks and no β relaxation peak.

According to Khanna et al. the magnitude for the β relaxation tended to increase mostly with the increase in amorphous volume and the dispersion peak temperature (T_β) increased with increasing molecular weight and was influenced by the type and amount of branching [32]. In order to confirm the β relaxation peak, the temperature dependence of E' and E'' at a frequency of 10 Hz was obtained for melt films of branched polyethylene, G201 and G808 with crystallinity <46%. Fig. 8 shows the results. A dispersion peak associated with the β relaxation can be surely observed around −25 °C but no α dispersion can be observed obviously. Here we must emphasize that the peak is associated with the β relaxation, since positron annihilation provides the second transition of τ_3 which appears at −30 °C. The detailed analysis shall be discussed later in this paper. Based on this information, the frequency dependence of E' and E'' was measured in the temperature range from −80 to 10 °C and the master curves of E' and E'' were constructed only by shifting horizontally, reduced to the common reference temperature of −20 °C.

Fig. 9 shows the Arrhenius plots for G201 and G808. The activation energies are given as 114 kJ/mol for G201 and

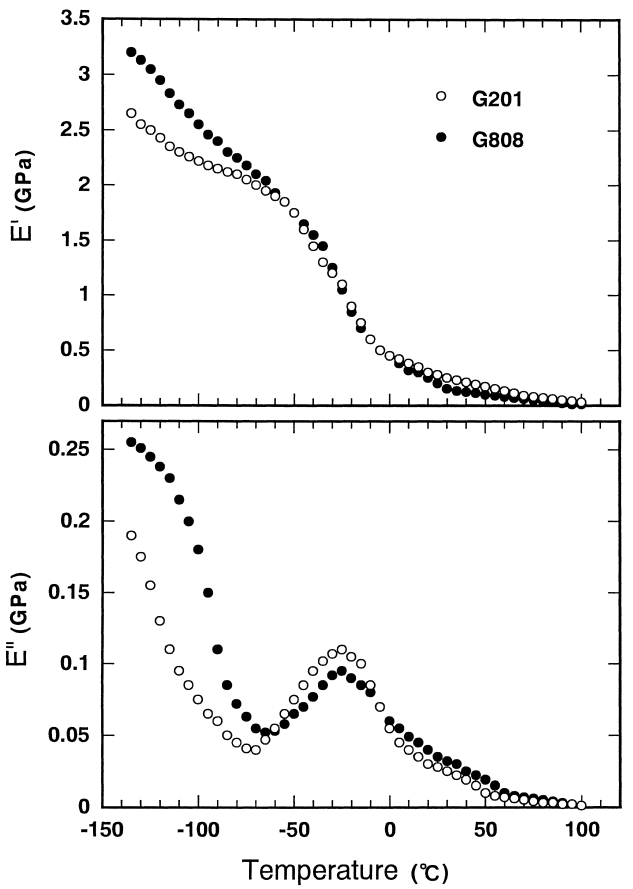

Fig. 8. Temperature dependence of the complex dynamic moduli at a frequency of 10 Hz for the melt films of G201 and 808.

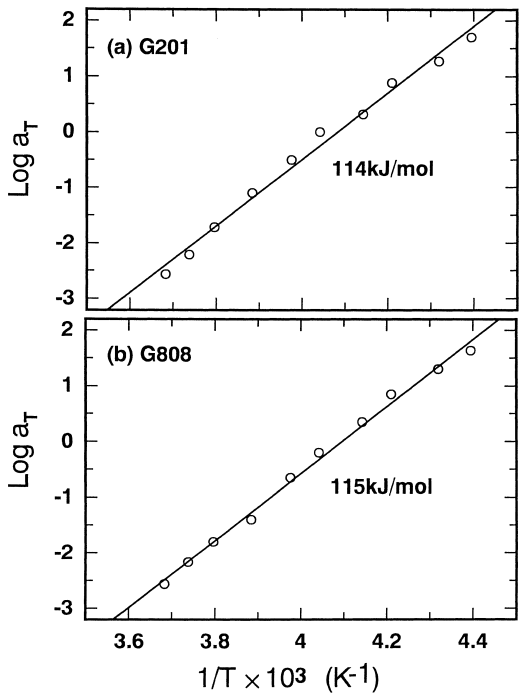

Fig. 9. Arrhenius plots of the horizontal shift factor $a_T(T, T_o)$ for G201 and G808 films.

115 kJ/mol for G808. The values between the two specimens are almost equal in spite of different melt indices as mentioned in Section 2. Khanna et al. proposed that the β relaxation mechanism is the glass transition [32]. The activation energy of the β relaxation estimated by dynamic X-ray measurements, however, was almost equal to that of the α_1 relaxation relating to intra-lamellar grain boundary phenomena associated with reorientation of crystal grains between the lamellae within spherulites. Because of the activation energy higher than 100 kJ/mol, the β mechanical relaxation cannot be assigned to the glass transition. According to the concept of Kawai et al. [26], the distinction between the α_1 and β mechanical relaxations of G201 with low crystallinity was reported to be impossible from the activation energies, since the both energies were almost the same. In their report, the energy of the β relaxation for linear polyethylene films became lower as crystallinity increase and the activation energy became less than 100 kJ/mol and the both relaxations could be discriminated.

In accordance with refined works for HDPE by Hentschel et al. [30], chain motion in the amorphous phases (HDPE) and glass transition were studied by using ^{2}H NMR [16], and the change of ^{2}H spectra measured in temperature range from −163 to 37 °C was analyzed in terms of free volume picture relating to thermal expansion in the amorphous region. They pointed out that increasing free volume provides an increase in the number of conformations accessible to molecular motion. They suggested three bond motions at low temperatures, five-bond motions at room temperature and motions with more than 10 bonds below the melting point.

An increase in free volume can be clearly estimated by positron annihilation [61]. Positron annihilation is one of the useful techniques to investigate characteristics of polymers. One can notice such a phenomenon that as positrons emitted from ^{22}Na induce radiation damage, the intensity (I_3) of the long-lived component of ortho-positronium (*o*-Ps) tends to decrease gradually with the measurement times [62,63]. The decrease of I_3 depends on the kinds of polymer and the positron irradiation effect occurs mostly in the amorphous phase. According to several reports [44–47], the effect provides an interesting probe at low temperatures to study positronium formation and the characteristics of polymers. For example, I_3 tends to increase with decreasing temperature and this tendency had been explained by the relaxation of the polymer structures by a number of studies [64].

Fig. 10 shows the intensity I_3 and the lifetime τ_3 of positronium as a function of temperature. The calender film (linear PE with $\lambda = 3$) and undrawn melt film (branched PE, G201) were used as test specimens. The cooler the sample became, the greater was the increase in I_3. This tendency has been confirmed for other samples [65]. The increase in I_3 is due to accumulation of trapped electrons in shallow traps, which are created after freezing the molecular motions at low temperature and attains saturation. As can be seen in this figure, around −120 °C, I_3 begins to decrease with increasing temperature and attains to a minimum at −30 °C. −120 °C was considered to be the temperature corresponding to the local mode relaxation of polyethylene having two effects on the trapped electrons: the commencement to remove trapped electrons from the shallow potential and the contribution to the elimination of the shallow potential due to the motion of polymer chains.

In accordance with Suzuki et al., the local motion around −30 °C causes a large movement of polymer chains and most of shallow potentials may be smeared out by the movement and then the trapped electrons may also disappear [66]. If this is the case, the molecular motion at low temperatures affect the trapped electrons in shallow potential and consequently the variation of I_3 is closely related to the relaxation temperature as a secondary effect. Beyond −30 °C, I_3 increases again. This is due to the fact that very small holes, which cannot be detected by positron annihilation, can be detected by an increase in the size of the holes upon thermal expansion. Consequently, it turns out that the β dispersion corresponds to the minimum point of I_3 and the γ dispersion, the starting point of the decrease in I_3.

On the other hands, the lifetime τ_3 is well-known to be related to the size of hole by using Tao's equation [61]. The longer τ_3, the bigger the hole size in polymer solid. As shown in Fig. 10, there exist three transitions of τ_3. for the branched polyethylene film G201. The first transition corresponds to the glass transition (the γ relaxation) associated with an increase in free volume, and the second transition at −30 °C corresponds to the β relaxation. The third transition at 50 °C is attributed to the onset of molecular motions in the epidermis part of crystallites

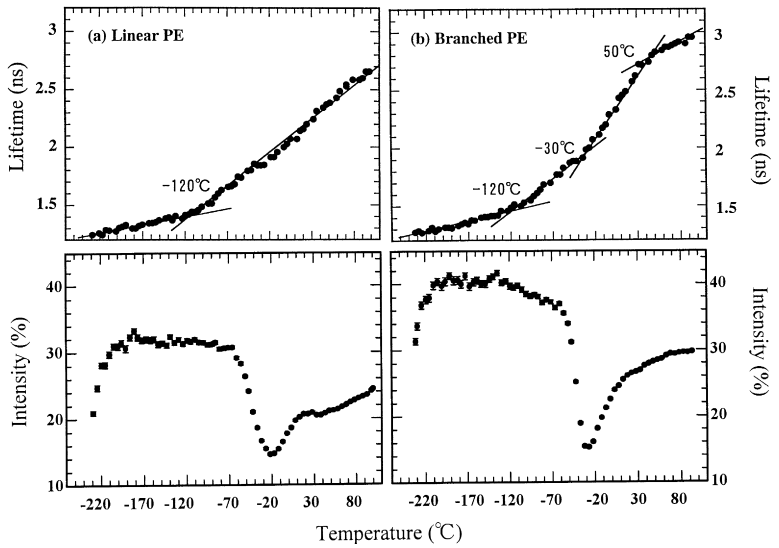

Fig. 10. Lifetime (τ_3) and intensity (I_3) against temperature for the calender film (linear PE) and the indrawn melt film (branched PE).

corresponding to the grain boundary regions. The transitions of τ_3 show a good correlation with the varying behavior of I_3. This result supports that the peak of E'' around -25 °C in Fig. 8 is surely the β relaxation associated with a large movement (macro-Brownian motion) of amorphous chains. On ther other hand, there is only the first transition for a linear polyethylene film with $\lambda = 3$. No appearance of the second peak supports no peak of β relaxation in Fig. 1(b). This tendency is also confirmed for the ultradrawn polyethylene [67].

Returning to Figs. 4(a) and 7(a), it is seen that there exist two kinds of activation energy indicating two components of the γ relaxation: 25 and 10 kJ/mol for the calender film ($\lambda = 3$), 25 and 11 kJ/mol for the calender film ($\lambda = 14$), 24 and 9 kJ/mol for the undrawn fiber (mono-filament) and 23 and 10 kJ/mol for the drawn fiber. Interestingly, the two kinds of activation energies are independent of the molecular orientation, crystallinity and mechanical property in bulk, although the orientation of crystallites for the undrawn and drawn fibers are quite different each other as shown in Table 2. This result supports the concept that the γ relaxation is associated with the local motion of molecules as discussed before. Based on ^{13}C NMR measurements for polyethylene, Kitamaru et al, pointed out that the non-crystalline component can be classified into two regions: a rubber-like amorphous component and an interfacial noncrystalline one [68]. Their concept was verified for several kinds of polyethylene films [69]. The activation energy, 9–10 kJ/mol is similar to the rotational barrier for the central C–C bond in *n*-butane reported to be about 13.8 kJ/mol from thermodynamic data [70,71]. If this is the case, the relaxation with the activation energy, 9–10 kJ/mol, is thought to be due to the local rotational barrier of central C–C bond in rubber-like amorphous phase associated with no significant intermolecular potentials. In contrast, the activation energy, 23–25 kJ/mol, suggests high rotational barrier relating to local motions of the central C–C bond within the interfacial-like amorphous phase. Accordingly, the γ relaxation mechanisms with activation energies, 9–10 and 23–25 kJ/mol are termed as the γ_1 and γ_2, respectively, and the detailed discussion shall be done together with nuclear magnetic relaxation.

The serious problem to pursue the detailed discussion is due to the different measurement conditions between the complex moduli and ^{13}C NMR. The complex moduli were obtained with a fixed length by clamping the film between two metallic clamps, while the ^{13}C NMR data were obtained with the length which allowed the change freely during the measurement at elevated temperature. In our NMR instrument, it was impossible to set the specimen with fixed length in the cylinder type sample tube. To check the temperature dependence of crystallinity under the measurement process of the complex moduli, the crystallinity was estimated by X-ray diffraction measured with a fixed length.

Fig. 11 shows X-ray diffraction intensities as a function of s ($s = 2\pi \sin\theta_B/\lambda'$, where θ_B is the Bragg angle and λ' is the wavelength of X-ray) for the quenched G201 at the indicated temperature. The curves were obtained by subtracting the air scattering, polarization absorption, and incoherent scattering from the observed intensity. The dotted line represents the contribution from the non-crystalline phase after subtracting the summation of intensity curves of each crystal plane. Ruland [72–74] and Killian [75] proposed the method to estimate crystallinity of a random orientation system from X-ray diffraction intensity curve and their method is applied to an oriented system in this paper. In the oriented system, the crystallinity can be obtained as follows:

$$X_{cr}(T) = X'_{cr}(T)K \quad (1)$$

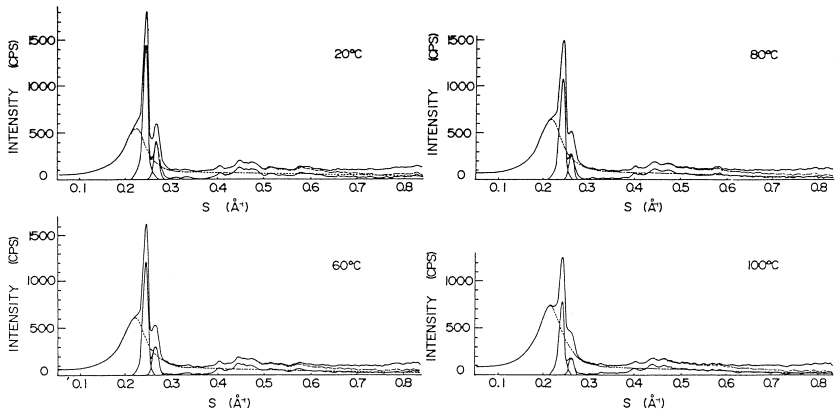

Fig. 11. X-ray diffraction intensity as a function of s for G201.

where $X_{cr}{}'(T)$ and K are given by

$$X'_{cr}(T) = \frac{\int_0^{\frac{\pi}{2}} \int_{S_0}^{S_p} s^2 I_{cr}(s,\theta,T) \sin\theta \, ds \, d\theta}{\int_0^{\frac{\pi}{2}} \int_{S_0}^{S_p} s^2 I(s,\theta,T) \sin\theta \, ds \, d\theta} \tag{2}$$

and

$$K = \frac{\int_{S_0}^{S_p} s^2 \langle f^2 \rangle ds}{\int_{S_0}^{S_p} s^2 \langle f^2 \rangle D_t^2 ds} \tag{3}$$

where

$$\langle f^2 \rangle = \frac{\sum n_j f_j^2}{\sum n_j} \tag{4}$$

$I_{cr}(s,\theta,T)$ and $I(s,\theta,T)$ in Eq. (2) are the intensity distributions from the crystallites and the specimens, respectively, at θ denoting the polar angle between the reference axis and stretching direction. The actual measurement was carried out by rotating about the film normal direction at 10° intervals of θ from 0 to 90° and the X-ray diffraction curve as a function of s was obtained at each θ. This means that the estimation of crystallinity of the drawn film is much more complicated than that of an undrawn film, since the integration of Eq. (2) over θ is unnecessary for random system. Because of the difficult measurements, the estimation of crystallinity using above method has never been reported. S_0 is the value associated with the initial scanning angle and S_p is related to the desired scanning angle for determining the crystallinity. f_j is the scanning factor of the jth atom and n_j is the number of atoms within a crystal unit. Therefore, $\langle f^2 \rangle$ is the average scattered intensity from the atoms. D_t is the coefficient containing the first- and second-order lattice distortion associated with thermal fluctuation, which is given by

$$D_t^2 = \exp\{-ks^2\} \tag{5}$$

Table 3 shows the temperature dependence of crystallinity of G201 films and Tables 4 and 5, the calender films with $\lambda = 3$ and 14. The value of k in Eq. (5) must be determined to give a constant value of crystallinity which is independent of the integrated region ($S_p - S_0$). Such a value was chosen by computer. The crystallinity decreases with increasing temperature but the values at room temperature are almost equal to those measured by density shown in Table 1.

To check the difference of temperature dependence of crystallinity between X-ray and ^{13}C NMR, CP/MAS spectra were measured for G201 at temperatures from 30 to 100 °C. Fig. 12 shows the results. The mass fraction is sensitive to an increase in temperature. The magnitude of the peak intensity decreases with increasing temperature, although the CP/MAS spectra emphasize the contribution of crystalline phase. The contribution from crystalline phase disappeared at 100 °C. This is quite different from the data obtained by X-ray diffraction shown in Fig. 11 and Table 3, since the crystallinity at 100 °C was more than 35%. The large difference between X-ray and ^{13}C NMR is probably due to the different experimental conditions as discussed already. Of course, this suggests that much caution should be exercised in comparing the results obtained by the dynamic mechanical measurements, positron annihilation and ^{13}C NMR.

In spite of the detailed analysis discussed already, it is not yet clear how the motion of individual carbons in the molecules contributes to these relaxation processes. Variable-temperature ^{13}C high-resolution NMR in solids has

Table 3
Crystallinity for the quenched G201 film calculated by a desired value of k (0.5) to give a constant value in the intergated region of S_0 to S_p using the Ruland method

Integrated region S_0–S_p	Temperature (°C)				
	20	40	60	80	100
0.1–0.495	49.0	45.8	40.8	37.7	37.0
0.1–0.555	47.7	44.9	41.2	37.6	37.6
0.1–0.620	48.6	44.6	41.8	38.4	37.7
0.1–0.680	47.9	44.0	40.9	38.2	36.3
0.1–0.750	47.5	44.7	41.2	39.8	36.2
0.1–0.805	46.8	45.5	41.7	40.4	36.5
Average (%)	47.8	45.1	41.4	39.0	36.4

Table 4
Crystallinity for calender film at $\lambda = 3$ calculated by a desired value of k (0.5) to give a constant value in the integrated region of S_0 to S_p using the Ruland method

Integrated region S_0-S_p	Temperature (°C)				
	20	40	60	80	100
0.1–0.495	68.8	67.1	65.3	63.1	57.6
0.1–0.555	67.8	67.1	65.5	63.7	58.3
0.1–0.620	69.5	67.6	67.2	62.8	59.7
0.1–0.680	68.7	66.8	67.3	64.4	59.5
0.1–0.750	69.0	67.1	67.1	64.5	59.5
Average (%)	68.8	67.1	66.5	63.7	58.9

played an important role to analyze the relaxation processes whose parameters can be measured for each carbon by combining the techniques of cross polarization, high-power proton decoupling, and magic-angle sample spinning [34–36].

For the above glass transition temperature T_g, ^{13}C high-resolution spectra are obtainable even for solid polymers by conventional NMR spectrometers used for liquids owing to the relaxation of $^{13}C-^{1}H$ dipolar interactions by rapid molecular motions. Horii et al. [38] studied molecular motions of each constituent carbon in different polyesters above T_g by the determination of ^{13}C spin–lattice relaxation time T_{1C}. On the basis of the same concept, local dynamics in bulk poly(vinyl methylether) was investigated by Dejean [39]. They pointed out that the molecular motions in bulk are of the same nature in solution and the local motions observed by NMR belong to the glass transition on the basis of the similarity of the temperature variation of the correlation time concerning conformational jumps to the predictions of the WLF equation for visco-elastic relaxation [76]. Mohanty et al. measured T_{1C} as a function of temperature for poly (γ-*n*-octadecyl L-L-glutamate) (POLG) and poly (γ-*n*-octadecyl L-glutamate) (POLLG) to analyze molecular motion of polyglutamate. For POLG, they observed a clear minimum value of T_1 for POLLG

Table 5
Crystallinity for calender film at $\lambda = 14$ calculated by a desired value of k (0.5) to give a constant value in the integrated region of S_0 to S_p using the Ruland method

Integrated region S_o-S_p	Temperature (°C)				
	20	40	60	80	100
0.1–0.495	87.9	87.0	87.7	85.5	80.0
0.1–0.555	87.2	85.9	87.1	84.5	79.2
0.1–0.620	87.9	86.3	87.6	85.0	80.2
0.1–0.680	87.5	86.5	87.5	84.6	80.9
0.1–0.750	87.6	86.8	87.6	84.7	81.2
Average (%)	87.6	86.5	87.5	84.9	80.3

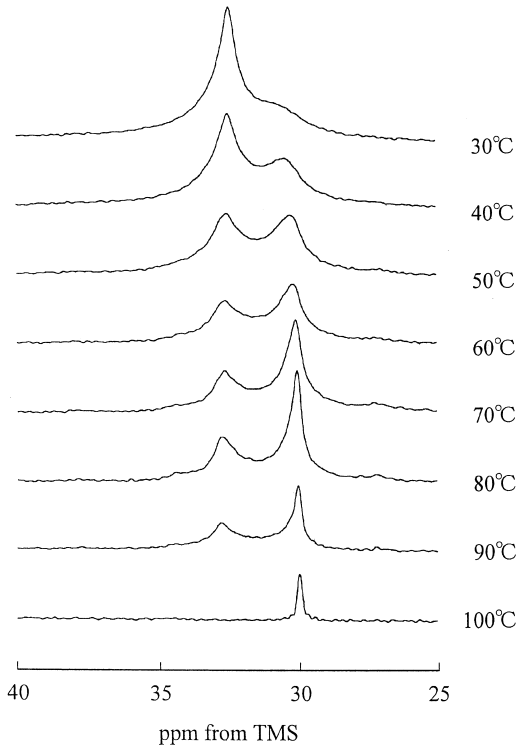

Fig. 12. CP/MAS spectra measured for G201 at the indicated temperatures.

associated with the β relaxation at 0 °C and a shoulder associated with the γ relaxation at −40 °C [40].

Recently, Chen et al. reported the ^{13}C spin–lattice relaxation times, T_{1C} of ^{13}C-labeled polyethylene crystallized under different conditions at temperature from −120 to 44 °C to study dynamics of the non-crystalline region [41]. They obtained T_{1C} for the non-crystalline component which appears at 30.3 ppm. According to their paper [41], the minimum value of T_{1C} occurs around −10.5 °C for the solution-crystallized specimen and around −30.5 °C for the melt-crystallized specimen. Their activation energies for the former and latter specimens were estimated to be 21.7 and 15.6 kJ/mol, respectively, by assuming a single relaxation mode. Based on the values, they pointed out that the relaxation is due to rapid *trans-gauche* transition in the amorphous phase. Surely, the relaxation with 15.6 kJ/mol is similar to the rotational energy (13.8 kJ/mol) around the central C–C bond of *n*-butane but the other relaxation with 21.7 kJ/mol is obviously out of the framework of the rotational barrier in the rubbery-like amorphous phase.

To obtain the further detailed analysis of the relaxation mode of polyethylene, the local relaxation mode is also investigated by ^{13}C NMR. In doing so, T_{1C} and the mass fractions were measured by Torchia's pulse sequence and by DD/MAS, respectively, for G201 and G808 at room temperature. To obtain T_{1C} of the orthorhombic crystal form for each specimen, the semi-logarithmic plot of the peak height of line 33 ppm was done against decay time τ_c. The DD/MAS spectra, which reproduce the contribution from all structural components, were obtained after the T_{1C}

measurement, since the waiting time was chosen to be longer than five times against the longest T_{1C} for G201 and G808. Each spectrum was analyzed by the least-square fitting in terms of three parameters of the complex function given as Gaussian and Lorentzian functions, in which the line width and peak height of each component were determined on the basis of small changes from the initial peak position. As listed in Table 6, the orthorhombic crystal form is made up of three components with different T_{1C} values with significant ranges of variability as has been reported for several kinds of polyethylene samples [77]. The longest T_{1C} values listed in Table 6 are much lower than those reported for single crystal mats and dry gel films with crystallinity $>80\%$. Of course, it is incorrect to assign the shortest T_{1C} values, 0.45 s for G201 and 0.70 s for G808, as the noncrystalline component, although the value is fairly in good agreement with a single value of T_{1C} (0.305 s) of the non-crystalline component measured by the standard saturation recovery pulse sequence.

The DD/MAS spectrum gave the mass fractions, in which the total mass fraction of orthorhombic and monoclinic crystal forms can be estimated as the crystallinity. In this case, the values for G201 and G808 are 49 and 47%, respectively and they are in good agreement with the crystallinity estimated from the density measurement. As has been reported for polyethylene samples, there exist two components in the non-crystalline regions; a rubbery component and a less disordered component. The latter is thought to be located in the interfacial region (not paracrystalline) between the crystalline and rubbery components. The difference between the two components, however, cannot be detected by X-ray diffraction. It will be discussed later in terms of temperature dependence of T_{1C}.

Fig. 13(a) and (b) shows partially relaxed spectra of G201 measured by the standard saturation recovery pulse sequence at 20 and -25 °C, respectively. At 20 °C, the contribution from crystalline components with $T_{1C} = 135$ and 7.5 s (see Table 6) is suppressed because of the short value of given τ. With increasing τ, the spectrum is postulated to contain all noncrystalline components and a part of the crystalline component with $T_{1C} = 0.45$ s. At -25 °C, the contribution from crystalline component disappeared at shorter values of τ than 0.5 s indicating

Table 6
^{13}C spin–lattice relaxation time (T_{1C}), crystallinity and amorphous fraction of G201 and G808 at room temperature

Specimen	T_{1C} (s)			Mass fraction (%)		
	Crystalline component orthorhombic			Crystalline	Interfacial	Rubbery
G201	135	7.5	0.45	49	32	19
G808	113	13.0	0.70	47	31	22

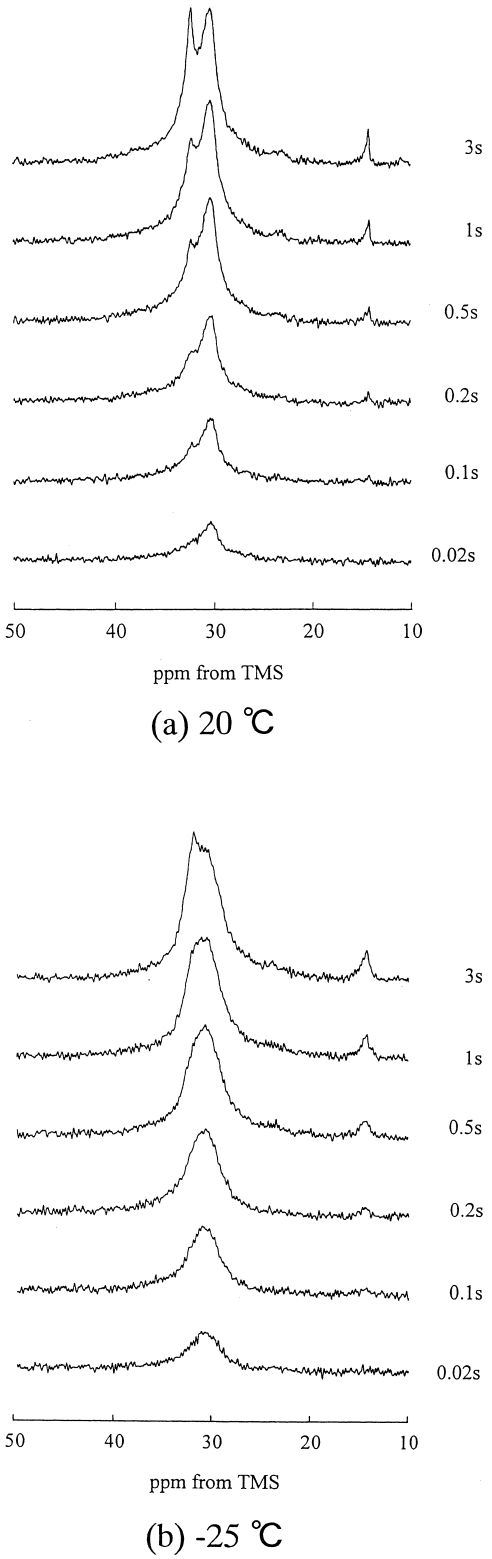

Fig. 13. Stacked spectra of the G201 as a function of τ by the standard saturation recovery pulse sequence.

that T_{1C} of the shortest component of the orthorhombic form at -25 °C is longer than that at room temperature.

Fig. 14(a) and (b) show the semi-logarithmic plot of the ^{13}C magnetization of the peak height of the non-crystalline

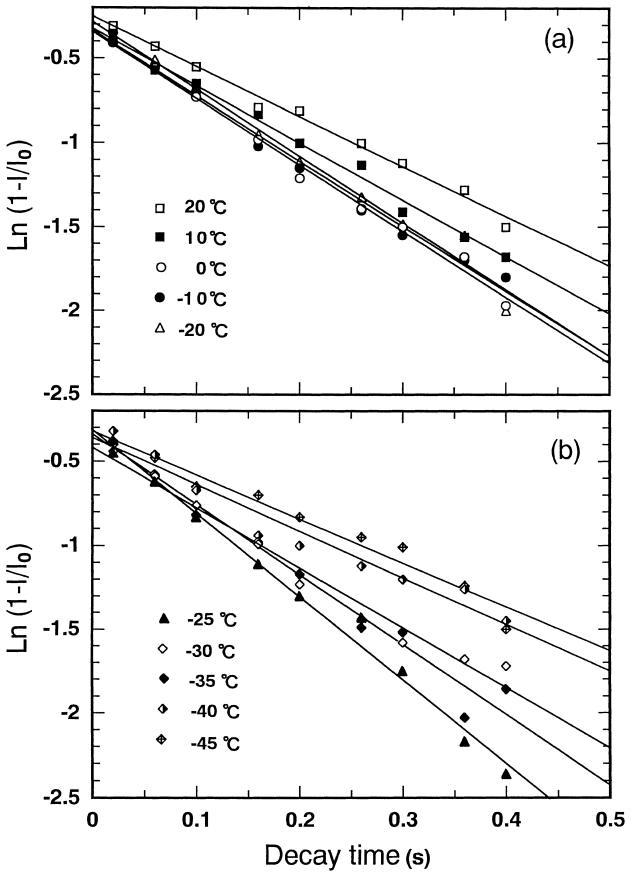

Fig. 14. Semi-logarithmic plot of the ^{13}C magnetization of the peak height of the non-crystalline component as a function of decay time.

component as a function of decay time τ_c by the standard saturation recovery method that is significant to estimate T_{1C} times shorter than a few seconds. The measurements were carried out in the temperature range from -45 to 20 °C. The decay curves showed one component. Above -25 °C, T_{1C} increases with temperature. This tendency was also confirmed even for ultra-drawn polyethylene with $\lambda = 300$ [27].

Fig. 15 shows the T_{1C} against the reciprocal absolute temperature. The minimum value of T_{1C} appeared around -25 °C corresponding to the β relaxation peak observed by the visco-elastic measurement shown in Fig. 8. By using the minimum value of T_{1C}, the relationship between T_{1C} and τ_c can be obtained by assuming a single correlation time model based on the BPP(Bloembergen, Purcell, Pound) theory [78]. If the temperature dependence of the correlation time τ_c follows the Arrhenius plots as $\tau_c = \exp(-\Delta E/RT)$, the activation energy ΔE can be estimated from the slope of $\ln(\tau_c)$ versus reciprocal absolute temperature $(1/T)$. The value is 20.7 kJ/mol and this value is higher than the value, 15.6 kJ/mol, obtained by Chen et al. [41]. Here it should be noted that this value is close to the value of activation energy, 23–25 kJ/mol, of the γ_2 relaxation by the dynamic mechanical measurements shown in Figs. 4(a) and 7(a). This supports that the activation energy estimated by ^{13}C

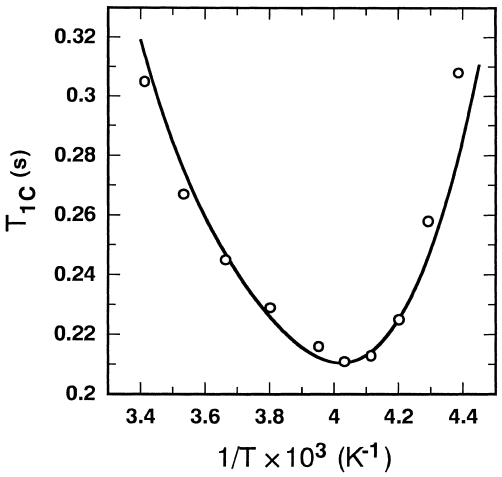

Fig. 15. Spin–lattice relaxation time T_{1C} against the reciprocal absolute temperature.

NMR is not related to the γ_1 but the γ_2 mechanism. Namely, the activation energy estimated by ^{13}C NMR is too high to assign as the γ_1 relaxation associated with the rapid *trans-gauche* transition in the rubbery-like amorphous phase, since the rotational barrier for the central C–C bond in n-butane is 13.8 kJ/mol. It is reasonable to consider that the dispersion at -25 °C by ^{13}C NMR belongs to the γ relaxation, although the dispersion at the same temperature measured by the dynamic mechanical measurements corresponds to the β relaxation. This adequacy is due to the large difference of frequency as the external applied excitation.

Because of the higher rotational barrier, the results by ^{13}C NMR and mechanical dynamic measurements together indicate that the γ_2 relaxation is associated with the motion of a short segment (e.g. three to four CH_2) as well as the local motion of loose chain ends within the interfacial-like amorphous phase. The curve in Fig. 16 is re-calculated from the activation energy ΔE. The curve is in good agreement with the experimental data indicating no existence of

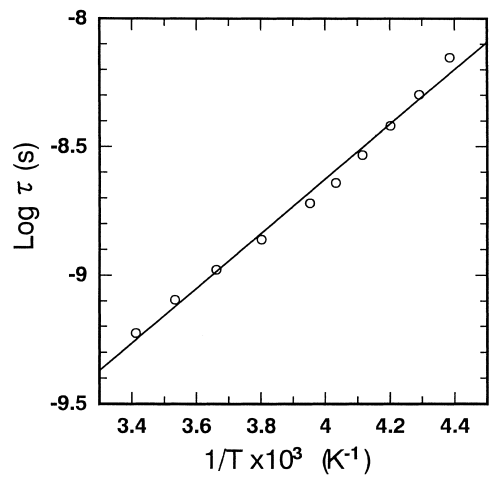

Fig. 16. Plots of correlation times τ_C of non-crystalline component against the reciprocal absolute temperature measured and recalculated for G201.

another minimum of T_{1C} at lower temperature < -25 °C associated with the γ_1 relaxation. Actually, as shown in Table 4, the mass fraction of interfacial component is much higher than that of rubbery component. Of course, we must consider the possibility that the result obtained from Fig. 16 represents the combined influence of the two correlation times.

Through a series of experimental results, it is evident that the rapid motion around the glass transition temperature invokes the γ relaxation and is independent of the β relaxation. It turns out that the β relaxation for undrawn films with spherulitic structure must be essentially similar to the mechanical dispersion of the α_1 dispersion. As discussed before, the β mechanical dispersion is assigned to large movement (macro Brownian motion) of amorphous chain while the α_1 mechanical dispersion is assigned to intra-lamellar grain boundary phenomena associated with reorientation of crystal grains within the lamellae pointed out by Kawai et al. [26]. In summary, dynamic X-ray diffraction is very powerful technique for studying the crystal dispersion (the α relaxation), while ^{13}C NMR and positron annihilation are powerful for studying the β and γ relaxation. Actually, any instrument except dynamic X-ray cannot distinguish the difference between α_1 and α_2.

4. Conclusion

Several relaxation processes of polyethylene were extensively investigated for specimens with different crystallinity, molecular orientation and superstructures by measuring dynamic mechanical relaxation, positron annihilation and nuclear magnetic relaxation. Three kinds of relaxation techniques were applied to the same specimen. For dynamic mechanical relaxation, the frequency dependence (from 0.01 to 100 Hz) of their complex dynamic tensile modulus was measured in the range of temperature from -150 to 130 °C. The master curves were constructed by shifting horizontally and then vertically. From the Arrhenius plots, the activation energies of the α_1 and the α_2 relaxations were determined to be 97–118 and 141–176 kJ/mol, respectively. The activation energies of the α_1 and α_2 relaxations become smaller with increasing draw ratio. This phenomenon was in good agreement with the results of rheo-optical studies reported already. The activation energy of the β relaxation was 114–115 kJ/mol. These values were similar to those of the α_1 relaxation. Because of the similar value of the activation energy, it is obvious that the β mechanical relaxation cannot be assigned to the glass transition but to a large movement (macro Brownian motion) of amorphous chains. This result was supported by the temperature dependence of *o*-Ps lifetime measured by positron annihilation.

The relationship between lifetime and temperature suggested a glass transition around -120 °C corresponding to the γ relaxation mechanism. For the γ relaxation mechanisms, there exist two mechanisms, the γ_1 and γ_2, whose the activation energies are 9–11 and 23–25 kJ/mol, respectively. The activation energy of the γ relaxation is independent of the molecular orientation and crystallinity. The former value is similar to the rotational barrier for the central C–C bond in n-butane reported to be about 13.8 kJ/mol from thermal dynamic data. Accordingly, the activation energy, 9–11 kJ/mol, is thought to be due to the γ_1 relaxation associated with the rapid *trans-gauche* transition of a short segment (e.g., three to four CH_2) in the rubbery-like amorphous phase with no significant intermolecular potentials. The β and γ relaxations by the dynamic mechanical measurements were in good agreement with those estimated from the transition concerning lifetime as well as the intensity of the long-lived component of *o*-Ps.

For nuclear magnetic relaxation, the semi-logarithmic plot of the ^{13}C magnetization of the peak height of the non-crystalline component was done as a function of decay time by the standard saturation recovery method. The minimum value of T_{1C} appeared around -25 °C corresponding to the β relaxation peak observed by visco-elastic measurements. Assuming a single correlation time τ_c, the activation energy obtained was 20.7 kJ/mol, this value is close to the latter value of activation energy (23–25 kJ/mol) of the γ_2 relaxation by the dynamic mechanical measurement. The result by ^{13}C NMR did not provide two kinds of activation energies, which is thought to be due to combined influence of the two correlation times.

References

[1] Nakayasu H, Markovitz H, Plazek DJ. Trans Soc Rheol 1961;5:261.
[2] McCrum NG, Morris EL. Proc R Soc London 1966;A292:506.
[3] Takayanagi M, Matsuo M. J Macromol Sci Phys 1967;B1:407.
[4] Iwayanagi S, Miura I. Jpn J Appl Phys 1965;4:94.
[5] Tuijnman CAF. Polymer 1968;4:259.
[6] Stachurski Z, Ward IM. J Macromol Sci Phys 1969;B3:445.
[7] Manabe S, Sakado A, Katada A, Takayanagi M. J Macromol Sci Phys 1970;B4:161.
[8] Kagiyama T, Okada T, Katada A, Takayanagi M. J Macromol Sci Phys 1973;B7:583.
[9] Illers KH. Koll ZZ Polymer 1973;251:394.
[10] Arai H, Kuriyama I. Colloid Polym Sci 1976;254:967.
[11] Sinnot KH. J Appl Phys 1966;27:3385.
[12] Ashacraft CR, Boyd RH. J Polym Sci Polym Phys Ed 1976;14:2153.
[13] Boyd RH, Yemni TR. Polym Engng Sci 1979;14:1023.
[14] Sayre JA, Swanson SR, Boyd RH. J Polym Sci Polym Phys Ed 1978;16:1739.
[15] Bergman K. Koll ZZ Polymer 1973;251:962.
[16] Bergman K. J Polym Sci Polym Phys Ed 1978;16:1611.
[17] Schmidt-Rohr K, Spiess HW. Macromolecules 1991;24:5288.
[18] Hu WG, Boeffel C, Schmidt-Rohr K. Macromolecules 1999;32:1611.
[19] Kawaguchi T, Ito T, Kawai H, Keedy DA, Stein RS. Macromolecules 1968;1:126.
[20] Onogi S, Keedy DA, Stein RS. J Polym Sci 1961;50:153.
[21] Yamada R, Stein RS. J Appl Phys 1965;36:3005.
[22] Tanaka A, Chang E, Delf B, Kimura I, Stein RS. J Polym Sci Polym Phys Ed 1973;11:1891.

[23] Kyu T, Yasuda N, Suehiro S, Nomura S, Kawai H. Polym J 1976;8:565.
[24] Suehiro S, Yamada T, Kyu T, Fujita K, Hashimoto T, Kawai H. Polym Engng Sci 1979;19:929.
[25] Suehiro S, Kyu T, Fujita K, Kawai H. Polym J 1979;11:331.
[26] Kawai H, Suehiro S, Kyu T, Shimomura A. Polym Engng Rev 1983;3:109.
[27] Matsuo M, Sawatari C, Ohhata T. Macromolecules 1988;21:1317.
[28] Ogita T, Yamamoto R, Suzuki N, Ozaki F, Matsuo M. Polymer 1991;31:882.
[29] Hu WG, Schnidt-Rohr K. Acta Polym 1999;50:271.
[30] Hentschel D, Sillescu H, Spiess HW. Macromolecules 1981;14:1607.
[31] Nitta K, Tanaka A. Polymer 2001;42:1219.
[32] Khanna YP, Turi EA, Taylor TJ, Vickroy VV, Abott RF. Macromolecules 1985;18:1302.
[33] Crissman JM, Passaglia E. J Appl Phys 1971;42:4636.
[34] Crissman JM. J Polym Sci Polym Phys Ed 1975;13:1407.
[35] Schaefer J, Stejskal EO, Buchdahl R. Macromolecules 1977;10:384.
[36] Schaefer J, Stejskal EO. In: Levy GC, editor. Topics in carbon-13, NMR spectroscopy. New York: Wiley-Interscience; 1979. Chapter 4.
[37] Lyerla LR, Methods and experimental physics, vol 16.; 1980. Part A, Chapter 4.
[38] Horii F, Hirai A, Murayama K, Kitamaru R, Suzuki T. Macromolecules 1983;16:273.
[39] Dejean BR, Laupretre F, Monnerie L. Macromolecules 1988;21:2045.
[40] Mohanty B, Watanabe J, Ando I, Sato K. Macromolecules 1990;23:4908.
[41] Chen Q, Yamada T, Kurose H, Ando I, Shiono T, Doi Y. J Polym Sci Polym Phys 1992;30:591.
[42] Rosenkw K, Sillescu H, Spiess HW. Polymer 1980;21:757.
[43] Hentschel D, Sillescu H, Spiess HW. Polymer 1984;25:1078.
[44] Levey B, Lalovic M, Ache HJ. J Chem Phys 1989;90:3282.
[45] Zhang Z, Ito Y. Radiat Phys Chem 1991;38:221.
[46] Suzuki T, Oshima N, Miura T, Oki Y, Numajiri M. Polymer 1997;37:5521.
[47] Uedono A, Kawano T, Tanigawa S, Ban M, Kyoto M, Uozumi T. J Polym Sci Polym Phys 1997;35:1601.
[48] Wilchinsky ZW. J Appl Phys 1969;1960:31.
[49] Stein RS, Norris FH. J Polym Sci 1956;21:381.
[50] Bunn CW. Trans Faraday Soc 1939;35:482.
[51] Rhodes MB, Stein RS. J Polym Sci Part A-2 1969;7:1539.
[52] Stein RS, Rhodes MB. J Appl Phys 1960;31:1873.
[53] Illers VKH. Rheol Acta 1964;3:202.
[54] Hoffman JD, Williams G, Passaglia E. J Polym Sci Part C 1966;14:173.
[55] Nagamatsu K. Koll ZZ Polym 1960;172:141.
[56] Miki K, Hikichi K, Kaneko M. J Appl Phys 1967;6:931.
[57] Miki K, Yasuda J, Kaneko M. Jpn J Appl Phys 1969;8:159.
[58] Wada Y, Tsuge K. Jpn J Appl Phys 1962;1:64.
[59] Okano K. J Polym Sci Part C 1966;15:95.
[60] Matsuo M, Sawatari C. Macromolecules 1988;21:1653.
[61] Tao SJ. J Phys Chem 1972;56:5499.
[62] Walender M, Maurer FH. J Mater Sci Forum 1992;105:1181.
[63] Suzuki T, Oki Y, Numajiri M, Miura T, Kondo K, Ito Y. Radiat Phys Chem 1995;45:657.
[64] van Krevelen DW, Hoftyzer PJ. Properties of polymers. Amsterdam: Elsevier; 1976.
[65] Ito Y, Hirada T, Hamada E, Suzuki T, Ito Y. Acta Phys Pol A 1999;95(4):433.
[66] Suzuki T, Ito Y, Kondo K, Hamada E, Ito Y. Radiat Phys Chem 2000;58:485.
[67] Matsuo M, Ma L, Azuma M, He C, Suzuki T. Macromolecules 2002;35:3059.
[68] Kitamaru R, Horii F, Murayama K. Macromolecules 1986;19:636.
[69] Shimizu Y, Harashina Y, Sugiura Y, Matsuo M. Macromolecules 1995;28:6889.
[70] Pitzer KS. Ind Engng Chem 1944;36:829.
[71] Person WB, Pimental GC. J Am Chem Soc 1953;75:539.
[72] Ruland W. Acta Crystallogr 1960;13:1059.
[73] Ruland W. Polymer 1964;5:89.
[74] Ruland W. Acta Crystallogr 1961;14:1180.
[75] Killian HG. Koll ZZ Polym 1962;183:1.
[76] Williams ML, Landel RF, Ferry JD. J Am Chem Soc 1955;77:3701.
[77] Shimizu Y, Harashina Y, Sugiura Y, Matsuo M. Macromolecules 1995;28:6889.
[78] Bloembergen N, Purcell EM, Pound RV. Phys Rev 1948;73:679.